DRUG DISCOVERY

15(36), 2021

Molecular docking and dynamics simulation of L-hyoscyamine, eupatorium and alkaloid L27 as potential inhibitors against 3CLpro of SARS-CoV-2

Manisha Mandal[1], Shyamapada Mandal[2]✉

To Cite:
Mandal M, Mandal S. Molecular docking and dynamics simulation of L-hyoscyamine, eupatorium and alkaloid L27 as potential inhibitors against 3CLpro of SARS-CoV-2. *Drug Discovery*, 2021, 15(36), 181-201

Author Affiliation:
[1]Department of Physiology, MGM Medical College, Kishanganj-855107, India; E-mail: debmanisha@rediffmail.com
[2]Department of Zoology, Laboratory of Microbiology and Experimental Medicine, University of Gour Banga, Malda-732103, India; E-mail: sam.micro11@ugb.ac.in

✉**Corresponding author:**
Prof. Shyamapada Mandal, Laboratory of Microbiology and Experimental Medicine, Department of Zoology, University of Gour Banga, Malda-732103, India; Email: samtropmed@gmail.com

Peer-Review History
Received: 02 June 2021
Reviewed & Revised: 06/June/2021 to 23/August/2021
Accepted: 24 August 2021
Published: August 2021

Peer-review
External peer-review was done through double-blind method.

ABSTRACT

Background & objectives: The COVID-19 pandemic, caused with the infection of SARS-CoV-2, is long lasting, and there is no specific treatment for the disease. The current study authenticates, using bioinformatic approaches, the inhibition of SARS-CoV-2 3CLpro with three bioactive phytochemicals alkaloid L27, eupatorium and L-hyoscyamine from *Lycopodium clavatum*, *Eupatorium perfoliatum* and *Atropa belladonna*, respectively. *Methods:* Molecular docking, ADMET, drug-likeness analysis, molecular dynamics (MD) simulation, and free energy calculation were applied to 3CLpro interaction with alkaloid L27, eupatorium and L-hyoscyamine, for the determination of pharmacological efficacy, safety evaluation, to assess the dynamics and energetics of these complexes. *Results:* Molecular docking demonstrated binding energy ≤ -6.5 kcal/mol for the phytochemicals used as ligands. No violation of Lipinski's RO5, favourable ADMET properties and bioavailability scores (0.55) signify the suitability of drug-likeness for the selected ligands. Molecular dynamic simulation revealed the root mean square (RMS) deviation of ~ 0.12 nm about the protein backbone, and RMS fluctuations < 0.2 nm about the ligand-heavy atoms, indicating the stability of protein-ligand complex structures throughout the simulation course. *Interpretation & conclusions:* The key amino acid players in protein-ligand interactions were Lys5, Met6, Ala7 and Val125 through H-bond and hydrophobic bond formation. Though net binding free energy of 3CLPro with eupatorium (-121.36 kJ/mol) was more favorable than lycopodium (-114.17 kJ/mol) and L-hyoscyamine (-78.96 kJ/mol), all the ligands were found effective to inhibit the 3CLpro of SARS-CoV-2. Thus, the compounds alkaloid L27 from Lycopodium, eupatorium, and L-hyoscyamine might be useful in the management of COVID-19 associated symptoms.

Keywords: ADMET, *Atropa belladonna*, *Eupatorium perfoliatum*, *Lycopodium clavatum*, molecular docking, molecular dynamics simulation, SARS-CoV-2 3CLpro

DISCOVERY SCIENTIFIC SOCIETY

1. INTRODUCTION

The ongoing COVID-19 (coronavirus disease 2019) pandemic caused with SARS-CoV-2 (severe acute respiratory syndrome coronavirus 2) infection is a huge global health crisis, and there is an escalation of COVID-19 cases as well as deaths with an alarming rate because of the lack of COVID-19 specific effective drugs or suitable vaccines. Notably, as of April 28, 2021, 148,329,348 confirmed cases of COVID-19 including 3,128,962 deaths have been reported globally (https://covid19.who.int). Therefore, it is critical to discover the specific drugs, for the inhibition of SARS-CoV-2 growth and COVID-19 treatment, with improved efficacy and safety, and in this connection, different existing (approved and experimental) SARS-CoV-2 targetable drugs have been repurposed[1].

The SARS-CoV-2, on gaining entry into the host cell, with the help of receptor binding domain RBD of the spike protein S, releases its RNA, and translates the pp1a and pp1ab from ORFs 1a and 1b of the viral genome. The ORF1a encodes 3CLpro (3 chymotrypsin-like protease), also called main protease (Mpro) and the part of pp1a (nsp5), and PLpro (papain-like protease) that auto-catalyze the viral pp1a and pp1ab into 16 non-structural proteins (nsp1 to nsp16), the replicases, of which 11 are produced by the 3CLpro[2]. The SARS-CoV-2 3CLpro contains three domains: domain I (8-101 amino acid residues), II (102-184 amino acid residues) and domain III (201-306 amino acid residues), the substrate binding region is positioned at the cleft of domain I and II, consisting of conserved His41 (acts as nucleophile) and Cys145 (catalytic dyad that acts as a proton acceptor)[3]. The SARS-CoV-2 3CLpro is an excellent druggable target, because of its crucial role in cleaving the coronavirus polyproteins into functional components vital for viral replication and maturation, and there is no such enzyme produced in human with similar cleavage action that might exclude the possibility of cellular harmfulness upon the possible inhibition of 3CLpro[4].

In absence of an effective treatment of COVID-19 and in view of the adverse toxic effects of the currently available drugs, some phytoconstituents from medicinal plants are worthy of investigation for formulating suitable therapeutic strategies against COVID-19[5-6]. The bioinformatic tools like molecular docking, ADMET, drug-likeness analysis, molecular dynamics (MD) simulation, and free energy calculation are powerful tool in structure-based drug designing from protein-ligand interaction, estimation of pharmacological efficacy, safety assessment, to understand the dynamics and energetics of these complexes[7-8].

The homeopathic medicines, over the world, are mostly derivatives of plant products because of their safety and efficacy. The *Andgrographis paniculate* active compounds (andrographolide, 14-deoxy 11,12-didehydro andrographolide, neoandrographolide and 14-deoxy andrographolide), an excellent source of homeopathic medicine, have been shown to possess antiviral activity against 3CLpro of SARS-CoV-2 by molecular docking[8]. The Ministry of Ayush, Government of India has suggested for the treatment of COVID-19 with different homeopathic medicines, including belladonna, eupatorium and lycopodium (https://www.ayush.gov.in/ayush-guidelines.html). Treatment of laboratory confirmed acute COVID-19 cases with either *Bryonia alba*, *Gelsemium sempervirens*, *Arsenicum album*, or Phosphorus has been reported using different potencies (30 CH for 63%, 200 CH for 20%, and 5 CH to 10 M for 17% patients) with positive outcomes[9-10]. Moreover, a number of homeopathic medicines from India (http://ctri.nic.in/Clinicaltrials/advsearch.php; https://ayushportal.nic.in/Covid.aspx), along with *Natrum muriaticum* (LM2) has been in trial *(*Unique ID: UMIN000040602*) t*o investigate the effectiveness and safety of the drug for mild cases of COVID-19 in primary health care[11].

On the basis of the facts and findings mentioned above, the current study aims to perform computational validation, through molecular docking, ADMET analysis, MD simulation, and free energy studies, of three bioactive phytochemicals: alkaloid L27 from *Lycopodium clavatum*; eupatorium i.e., 2'-hydroxy-4,4',5',6'-tetramethoxychalcone from *Eupatorium perfoliatum*; L-hyoscyamine, a belladonna alkaloid from *Hyoscyamus niger* or *Atropa belladonna*, against SARS-CoV-2 target protein 3CLpro, for the management of COVID-19 using repurposed adjuvant homeopathic medicines.

2. MATERIALS AND METHODS

System information

The molecular docking and ADMET were analyzed in Windows 10 Pro Intel(R) Core (TM) i3-4010U CPU @ 1.70GHz, 4GB RAM, with Desktop 5IMLB7B 64-bit OS. MD simulation and free energy calculation were executed on Nvdia NV118 / Mesa Intel® UHD Graphics (ICL GT1), Cuda compilation tools, release 10.1, V10.1.243, 7.6 GiB memory, Intel® Core™ i5-1035G1 CPU @ 1.00GHz × 8 processor, with disk capacity 1.3 TB on Ubuntu 20.04.2 LTS 64-bit OS, 3.36.8 Gnome version.

Retrieval and preparation of ligands

The 3D structures of L-hyoscyamine (PubChem CID 3661), eupatorium (PubChem CID: 6253276), and alkaloid L27 (PubChem CID: 600064), were retrieved from PubChem (https://pubchem.ncbi.nlm.nih.gov/). The hydrogen atoms and Gasteiger charges were

ISSN 2278–540X EISSN 2278–5396 I OPEN ACCESS

added to the ligand using UCSF Chimera version 1.15 (https://www.cgl.ucsf.edu/chimera/). The residue names for the ligands L-hyoscyamine, eupatorium, and alkaloid L27 from lycopodium were EWBC, INMW and X7TW respectively, as available from Automated Topology Builder (ATB) and Repository version 3.0 (https://atb.uq.edu.au/).

Retrieval and preparation of protein

The crystal structure of SARS-CoV-2 3CLpro (PDB ID: 7K3T) was retrieved from RCSB PDB (http://www.rcsb.org//pdb). The ligands, solvents, or ions bound to the receptor were removed, and Gasteiger charges were added, using UCSF Chimera version 1.15 (https://www.cgl.ucsf.edu/chimera/). The active site of protein was predicted using fpocket 1.0, in RPBS (https://mobyle.rpbs.univ-paris-diderot.fr/cgi-bin/portal.py#forms::fpocket).

ADMET and drug-likeliness

The ADMET properties and bioavailability of ligands were evaluated using SwissADME (http://www.swissadme.ch/) and pkCSM (http://biosig.unimelb.edu.au/pkcsm/prediction). The oral drug likeness properties of the ligands were defined following Lipinski's RO5: molecular weight < 500 gm, lipophilicity log P < 5, hydrogen bond (H-bond) donors ≤ 5, H-bond acceptors ≤ 10, and molar refractivity < 140[12].

Molecular docking

The molecular docking of the ligands against 3CLpro were evaluated using AutoDock Vina, in UCSF Chimera 1.15 (https://www.cgl.ucsf.edu/chimera/download.html). A grid box of 30×30×30 $Å^3$ (for EWBC and X7TW) and 50×44×40 $Å^3$ (for INMW) were generated with coordinates: $x = 2.769$, $y = 2.776$, and $z = 24.065$, for all the ligands. The binding energy (BE) ≤ -6.5 kcal/mol was considered as the most binding effectiveness of the ligands with the receptor in the docking[13].

Ramachandran plot

For comparison and quality assessment of the structures, the protein and its complexes with the ligands were subjected to Ramachandran plot analysis with PROCHECK SAVES v6.0 (https://saves.mbi.ucla.edu).

Molecular dynamics simulation

To analyze the stability and dynamics of apo 3CLpro (without ligands) and halo 3CLpro (with ligands EWBC, INMW and X7TW), MD simulation was carried out for 1000 ps using GROMACS version 2021 (www.gromacs.org), with CHARMM36-feb2021 all-atom force field[14]. The topology for 3CLpro was built using GROMACS version 2021, and the topology parameterization of the ligands was carried out using CHARMM General Force Field (CGenFF) server[15]. A total of four simulations were performed: (i) 7K3T: model structure of 3CLpro without ligand, (ii) 7K3T-EWBC: model structure of 3CLpro complex with L-hyoscyamine, (iii) 7K3T-INMW: model structure of 3CLpro complex with eupatorium, and (iv) 7K3T-X7TW: model structure of 3CLpro complex with alkaloid L27 from Lycopodium.

The apo and halo 3CLpro were solvated individually in a dodecahedron box of size 10 Å with TIP3P water model. The solvated systems were neutralized with the addition of Na^+ ions. A convergence criteria of 1000 kJ/mol/nm were applied to achieve energy minimization for a maximum 50,000 steps to remove steric clashes (www.gromacs.org). Equilibration of the solvent molecules around the solute was applied on position restrained heavy atoms of the ligand along with the protein, using genrestr module of gromacs. Equilibration was conducted under isothermal-canonical (NVT) ensemble with constant number of particles N, volume V and temperature T, over 100 ps simulation period, using t couple = V-rescale (modified Berendsen thermostat) and Particle Mesh Ewald Coulomb for long range electrostatics[16-17]. Temperature coupling groups included protein-ligand and water-ions under protein and non-protein categories respectively. Equilibration of pressure P was achieved with isothermal-isobaric (NPT) ensemble for a 100 ps duration, wherein the number of particles N, P and T are constant, using Parinello-Rahman barostat[18]. The Van der Waals and Coulombic interaction cut-off radius utilized were 12 Å. The position restraining forces were released and MD simulation was conducted for 1000 ps using leap-frog integrator with time step of 2 fs, by searching neighbouring grid cells every 100^{th} step[19].

MD trajectory analysis

The MD trajectories were analysed to estimate the energies, intra-peptide and peptide-water hydrogen bonds, free energy of solvation, area per residue, solvent accessible surface area (SASA), root mean square deviation (RMSD) and RMS fluctuation (RMSF), using GROMACS version 2021 (www.gromacs.org) tools.

Binding Free Energy calculation

The binding free energies (ΔG_{bind}) were calculated applying Molecular Mechanics–Poisson Boltzmann Surface Area (MM-PBSA) approach[20] for the 3CLPro-ligand complex, given by, $\Delta G_{bind} = \Delta E_{electrostatic} + \Delta E_{VdW} + \Delta G_{solv} - T\Delta S$, where $\Delta E_{electrostatic}$, ΔE_{VdW}, ΔG_{solv}, and $T\Delta S$, correspond to the energy changes due to electrostatic and Van der Waals interactions, free energy change of solvation, and the entropic contribution $T\Delta S$ at temperature T. The entropy calculations were not done as they may alter the binding free energy values reported for the molecules[5].

Visualization

Molecular graphics and analysis of the protein-ligand complexes were done using VMD (http://www.ks.uiuc.edu/Research/vmd/), UCSF Chimera version 1.15 (https://www.cgl.ucsf.edu/chimera/download.html), XMGrace tools (www.gromacs.org), PyMOL version 2.4.1 (https://pymol.org), and Discovery Studio Visualizer v21. 1.0.20298 (https://discover.3ds.com/discovery-studio-visualizer-download).

3. RESULTS

ADMET analysis and drug-likeness

The EWBC, INMW and X7TW ligands obeyed Lipinski's RO5 for drug-likeness of a compound (Table I), and ADMET properties were within favourable ranges (Table II).

Table I. Lipinski's RO5 for the bioactive phytocompounds: EWBC, INMW, and X7TW interpreted with SwissADME and pkCSM

Property	Bioactive phytocompounds (ligand molecules)		
	EWBC	INMW	X7TW
Molecular Weight (g/mol)	289.37	344.36	261.36
LogP	1.9309	3.3227	1.757
#H-bond acceptors	4	6	3
#H-bond donors	1	1	1
Molar Refractivity	84.51	94.24	78.31
Fraction Csp3	0.59	0.21	0.81
#Rotatable bonds	5	7	0
TPSA (Å²)	49.77	74.22	40.54

EWBC: L-hyoscyamine; INMW: eupatorium; X7TW: alkaloid L27 from Lycopodium.

Table II. ADMET profiles of bioactive phytocompounds used as ligands (EWBC, INMW, X7TW)

Property	Model	Ligand molecules		
		EWBC	INMW	X7TW
Absorption	Water solubility (log mol/L)	-1.943	-4.434	-2.594
	Intestinal absorption (human) %	94.508	92.713	95.517
	Caco2 permeability	1.289	-4.434	-2.594
	Skin permeability (log Kp)	-4.488	-2.778	-3.514
	P-glycoprotein substrate	Yes	No	No
Distribution	Fraction unbound (human)	0.386	0	0.613
	BBB permeability (log BB)	0.234	-0.591	0.385
	CNS permeability (log PS)	-2.931	-2.968	-3.188
Metabolism	CYP2D6 substrate	No	No	No
	CYP3A4 substrate	No	Yes	Yes
	CYP3A4 inhibitor	No	Yes	No
Excretion	Total clearance (log ml/min/)	1.013	0.239	0.566
	Renal OCT2 substrate	No	No	No
Toxicity	AMES toxicity	No	Yes	No

ISSN 2278–540X EISSN 2278–5396 I OPEN ACCESS

Oral rat acute toxicity (LD_{50}) mol/kg	2.672	1.991	2.211
Oral rat chronic toxicity (LOAEL) log mg/kg bw/day	2.358	2.248	2.166
Hepatotoxicity	No	No	No
Skin sensitization	No	No	No

EWBC: L-hyoscyamine; INMW: eupatorium; X7TW: alkaloid L27 from Lycopodium

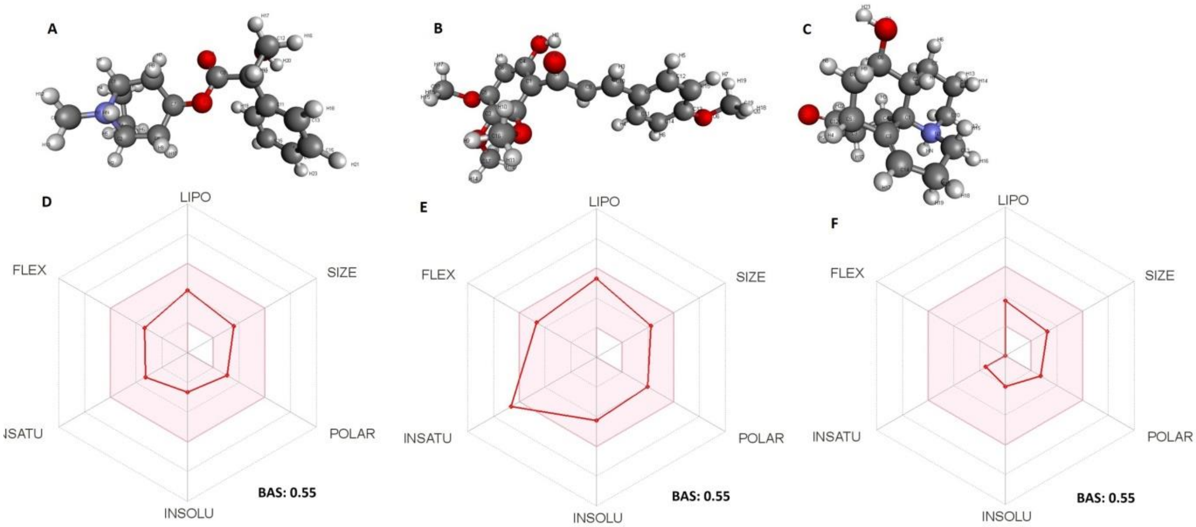

Fig. 1. 3D structure of ligands: (A) EWBC, (B) INMW, and (C) X7TW; bioavailability radar depicting LIPO (lipophilicity), SIZE (molecular weight), POLAR (TPSA: topological polar surface area), INSOLU (solubility), FLEX (flexibility), INSATU (saturation) and bioavailability score (BAS): (D) EWBC, (E) INMW, and (F) X7TW.

Molecular docking

The binding energies of EWBC, INMW and X7TW with 3CLpro were -6.9, -6.5 and -6.8 kcal/mol respectively. All the three ligands occupied similar binding sites within the pocket of 3CLpro (Fig. 2A). The 2D interaction in the docked complexes (Fig. 2B to 2G) showed 7K3T-EWBC complex displayed three conventional H-bonds with Gln110, Gln107 and Pro108, and 3 hydrophobic interactions (Fig. 2C). The 7K3T-X7TW complex showed three conventional H-bonds with Gln110 and His246, Gln107, and one hydrophobic bond with His246 (Fig. 2E). The 7K3T-INMW complex displayed two conventional H-bonds with His246, and 8 hydrophobic interactions (Fig. 2G). The 7K3T formed carbon-hydrogen bonds with Pro108, Gly109 and Glu240 for EWBC (Fig. 2C), Gly109, Gln110, Pro132 and Glu240 for INMW (Fig. 2G) and Pro108 for X7TW (Fig. 2E). The π-alkyl hydrophobic interaction was found with all the ligands; π-π stacked in EWBC and X7T; and π-π T-shaped and alkyl bonds in X7TW were found (Fig. 2). Electrostatic interactions involved attractive charge with Glu240 and π-cation with His246 in 7K3T-EWBC (Fig. 2C), and π-anion with Glu240 in 7K3T-X7TW (Fig. 2E).

Molecular dynamic simulation

The temperature attained ~ 300 K based on Maxwell distribution of kinetic energy, that remained stable during the equilibration period (Table III, Fig. 4A). The pressure with respect to a reference of 1 bar, fluctuated during equilibration, evident from large RMSD (Table III, Fig. 4B); application continued until the pressure reached the proper density (Table III, Fig. 4C), stable equal to the experimental value ~1000 kg/m^3 and expected density of TIP3P model value 980 kg/m^3.

The angles and the distances between the geometrical centres of donor-Hbond-acceptor (D-H···A) are depicted in Fig. 4D and Fig. 4E. The angle of gyration remained relatively unchanged about Cα (~110^0) and backbone atoms (~112^0) (Fig. 4f). The 7K3T remained stable in its folded conformation throughout simulation at 300 K, evident from invariant radius of gyration, average 2.19 nm (Fig 4E).

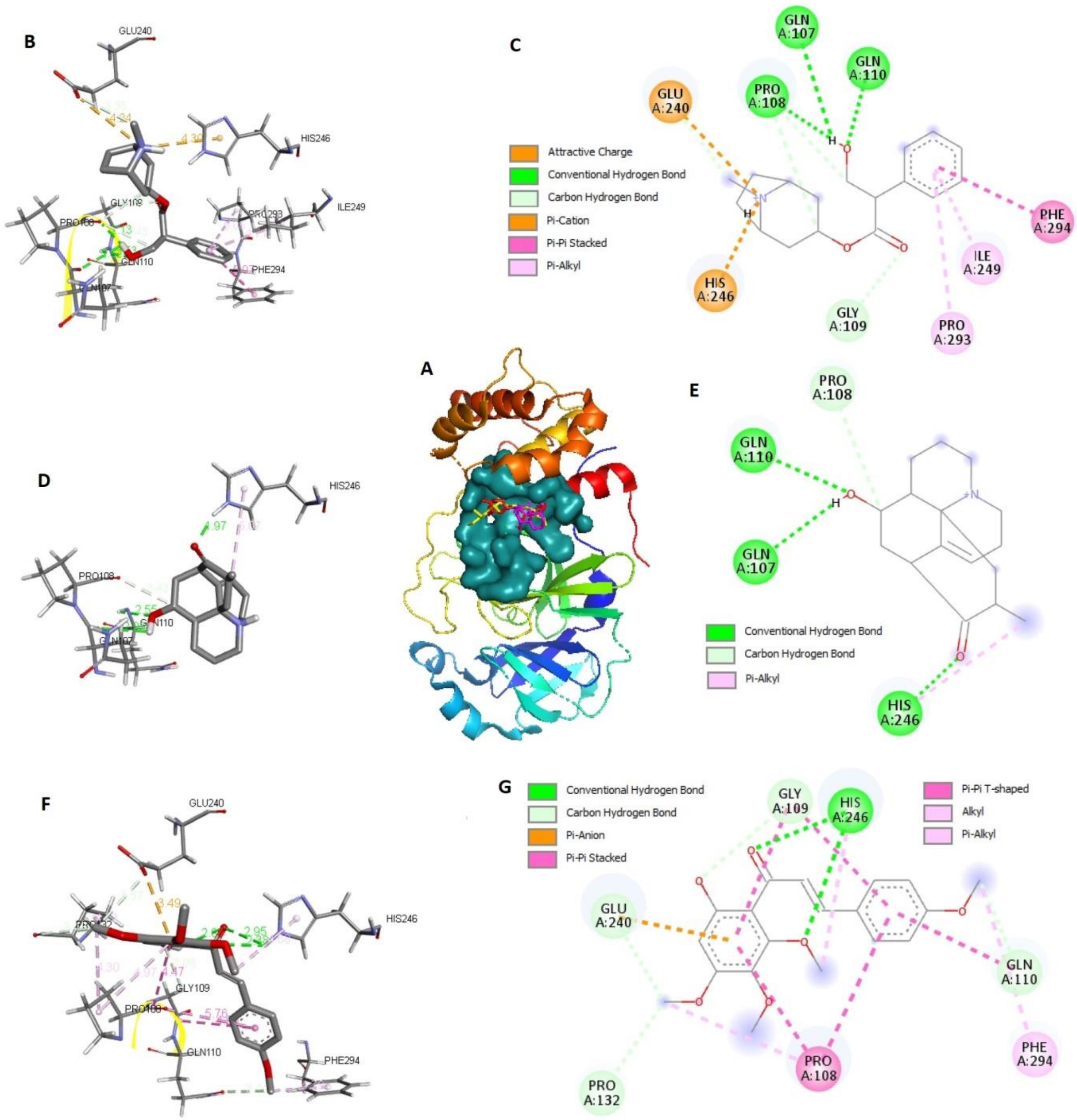

Fig. 2. (A) The poses of ligands EWBC (red), X7TW (magenta) and INMW (yellow) within the pocket of 3CLpro; 3D interaction of the docked complex: (B) 7K3T-EWBC, (D) 7K3T-X7TW, (F) 7K3T-INMW; 2D interaction of the docked complex: (C) 7K3T-EWBC, (E) 7K3T-X7TW, (G) 7K3T-INMW.

ISSN 2278–540X EISSN 2278–5396 I OPEN ACCESS

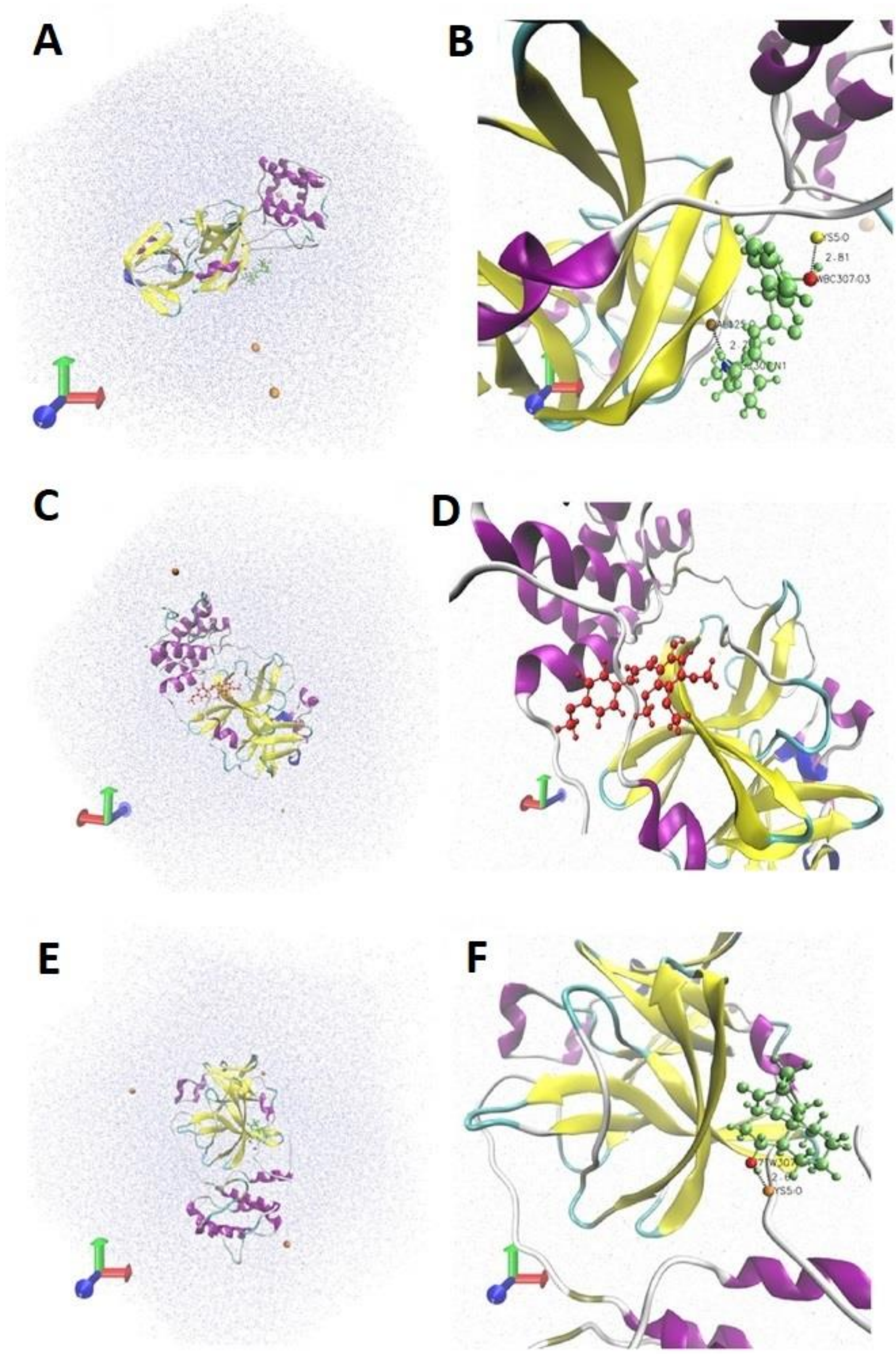

Fig. 3. VMD (visual molecular dynamics) of (A) 7K3T-EWBC, (C) 7K3T-INMW, (E) 7K3T-X7TW; key H-bond interactions in simulated complex: (B) 7K3T-EWBC, (D) 7K3T-INMW, (F) 7K3T-X7TW.

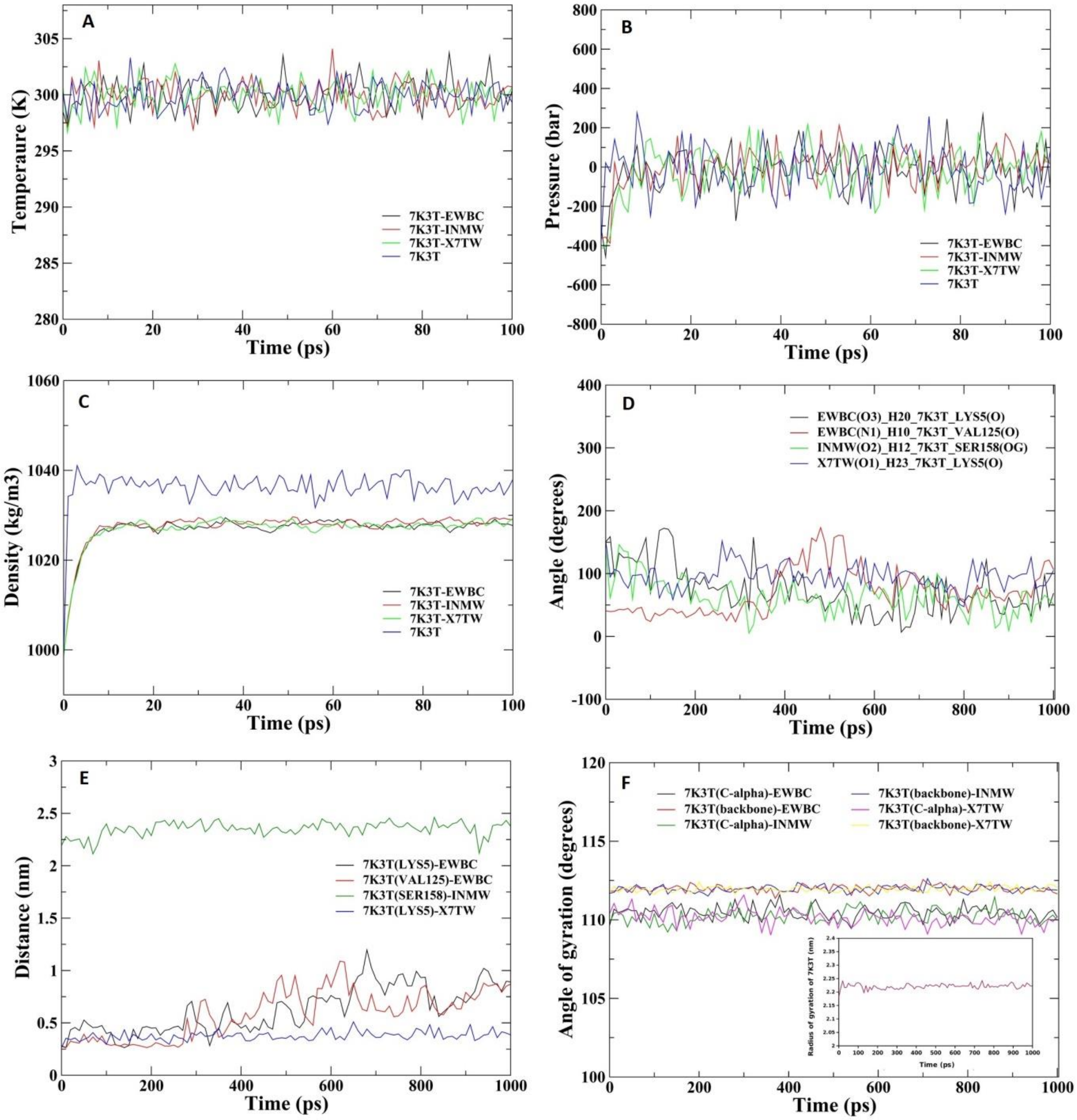

Fig. 4. Molecular dynamic trajectory analysis: (A) temperature progression over the course of simulation, (B) pressure variation with respect to the reference pressure of 1 bar, (C) equilibration with respect to density, (D) angle distribution, (E) distance between the geometrical centers of the important donor-Hbond-acceptor triplets, and (F) angle of gyration with radius of gyration of free protein in inset.

Table III. Energy parameters and structural features of ligand-bound and unbound protein 7K3T (3CLpro).

	7K3T-EWBC	7K3T-INMW	7K3T-X7TW	7K3T
Potential energy (kJ/mol)	-1.057×10^6	-1.024×10^6	-1.064×10^6	-1.022×10^6
Maximum force F_{max}	9.86×10^2on 4695 atom in 1043 steps	9.66×10^2on 1973 atom in 365 steps	8.84×10^2on 4697 atom in 1312 steps	8.57×10^2on 2063 atom in 313 steps
Solvent molecules (Na^+) number	21220 (3)	21219 (4)	21220 (3)	21232 (4)
Temperature (K)	299.77 ± 0.25	299.78 ± 0.15	299.74 ± 0.23	299.82 ± 0.21
Pressure (bar, RMSD)	-14.40 ± 9.9, 111.53	-12.50 ± 13.0, 109.40	-13.79 ± 13.0, 113.53	$-0.14.40 \pm 2.9$, 119.0
Density (kg/m3)	1026.97 ± 0.84	1027.50 ± 0.90	1027.03 ± 0.85	1036.37 ± 0.18

ISSN 2278–540X EISSN 2278–5396 I OPEN ACCESS

Enthalpy (kJ/mol)	-711677 ± 250	-711525 ± 190	-711337 ± 140	-721115 ± 100
Total interaction energy (kJ/mol)	-47.03 ± 5.2	-90.97 ± 1.5	-78.22 ± 1.0	_
C-SR (kJ/mol)	-11.58 ± 7.1	-28.64 ± 2.4	-24.34 ± 1.9	_
LJ-SR (kJ/mol)	-35.44 ± 7.5	-62.33 ± 1.8	-53.87 ± 0.8	_
RMSD (nm)	0.1283 ± 0.0194	0.1276 ± 0.0022	0.1176 ± 0.0016	0.1178 ± 0.0018(E) 0.1528 ± 0.0002(C)
Intra-peptide Hydrogen bonds	215.78 ± 0.69	223.14 ± 0.64	223.0 ± 0.66	222.84 ± 0.65
Peptide-water Hydrogen bonds	606.18 ± 1.20	586.58 ± 1.24	591.34 ± 1.25	585.54 ± 1.02
Total Hydrogen bonds	300	311	296	309
Total salt bridges	17	17	16	15
Ramachandran plot features				
G-factors				
(i) Dihedrals	-0.43	-0.41	-0.45	-0.19
(ii) Covalent	-1.74	-1.69	-1.67	-0.06
(iii) Overall	-0.94	-0.91	-0.93	-0.13
Planar groups				
Within limits	59.1%	53.6%	50.9%	93.6%
Highlighted	40.9%	46.4%	49.1%	64%
Residue properties				
Maximum deviation	4.6	4.9	5.0	4.0
Bond length/angle	7.3	7.9	7.1	5.2
Morris et al class	1 1 2	1 1 2	1 1 2	1 1 2
Bad contacts	0	0	0	0

7K3T-EWBC: 3CLpro complex with L-hyoscyamine; 7K3T-INMW: 3CLpro complex with eupatorium; 7K3T-X7TW: 3CLpro complex with alkaloid L27 from Lycopodium; 7K3T: 3CLpro without ligand; C: crystal; E: equilibrated; values expressed as mean ± SEM (standard error of mean)

RMSD and RMSF

The RMSD of backbone after least square fitting to backbone for apo and halo protein were ~0.12 nm throughout simulation (Fig. 5A). The RMSD of equilibrated and crystal structures over backbone atoms showed similar values (0.12 nm), implying stability of the structures. The RMSD of Cα after least square fit to Cα showed no deviation in structure compared to the backbone atoms. The RMSD about the backbone fitted to ligand heavy atoms were 0.4-0.5 nm (Fig. 5B). The RMSD of distances between backbone atoms were 0.09-0.10 nm, and ligand heavy atoms were 0.046, 0.056 and 0.011 nm, for INMW, EWBC and X7TW, respectively (Fig. 5C).

ISSN 2278–540X EISSN 2278–5396 I OPEN ACCESS

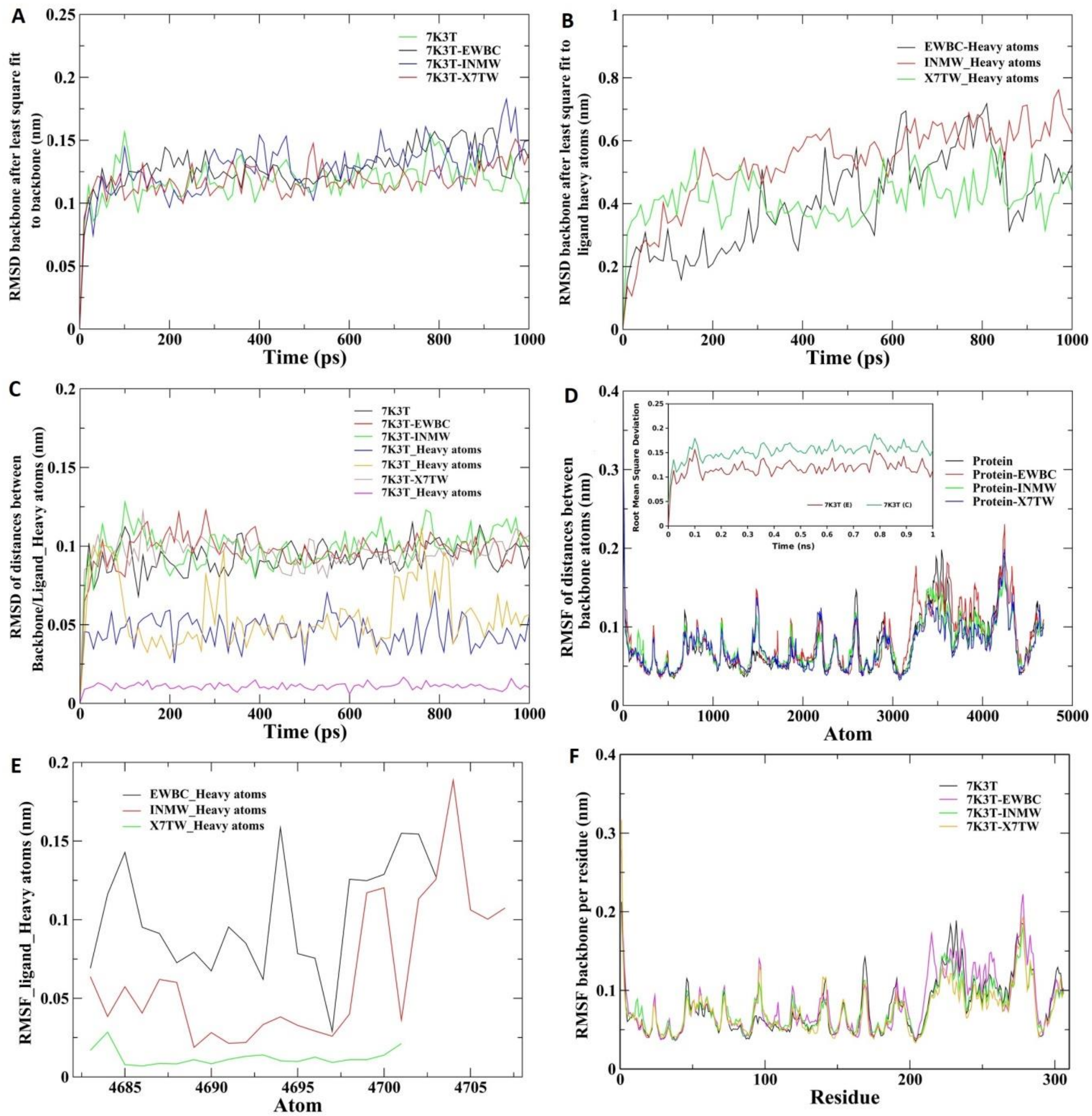

Fig. 5. Molecular dynamics RMSD and RMSF: (A) backbone RMSD after least square fit to backbone for the bound and unbound protein, (B) backbone RMSD fitted to ligand heavy atoms for the protein-ligand complex, (C) RMSD of distances between backbone atoms and between ligand heavy atoms, (D) RMSF of distances between backbone atoms, with RMSD of crystal 'C' and equilibrated 'E' structure for 7K3T in inset, (E) RMSF about the ligand-heavy atoms, and (f) RMSF per residue about the backbone atoms.

The RMSF of distances between backbone atoms showed no variation in structure with RMSD, except the crystal structure of the free protein (Fig. 5D). The RMSF of the ligand-heavy atoms remained < 0.2 nm (Fig. 5E). The RMSF per residue about the backbone atoms diminished from initial high values ranging 0.2-0.3 nm to an average of 0.07-0.08 nm levels (Fig. 5F).

Ramachandran plot and secondary structures

A relatively higher residue properties (maximum deviation and bond length/angle) and planar group features but lower G-factors (dihedrals and covalents) were observed in the protein-ligand complex compared to the free protein (Table III, Fig. 6A, 7A, 8A, 9A).

The evolution of visual molecular dynamics (VMD) attributed secondary structures including turn, extended configuration, isolated bridge, α-helix, 3-10 helix, Φ-helix and coil, categorized to each residue of the apo and halo 7K3T showed relative distribution of structures over the course of simulation with comparatively higher involvement of turns in fluctuation events (Fig. 6B, 7B, 8B, 9B).

ISSN 2278–540X EISSN 2278–5396 I OPEN ACCESS

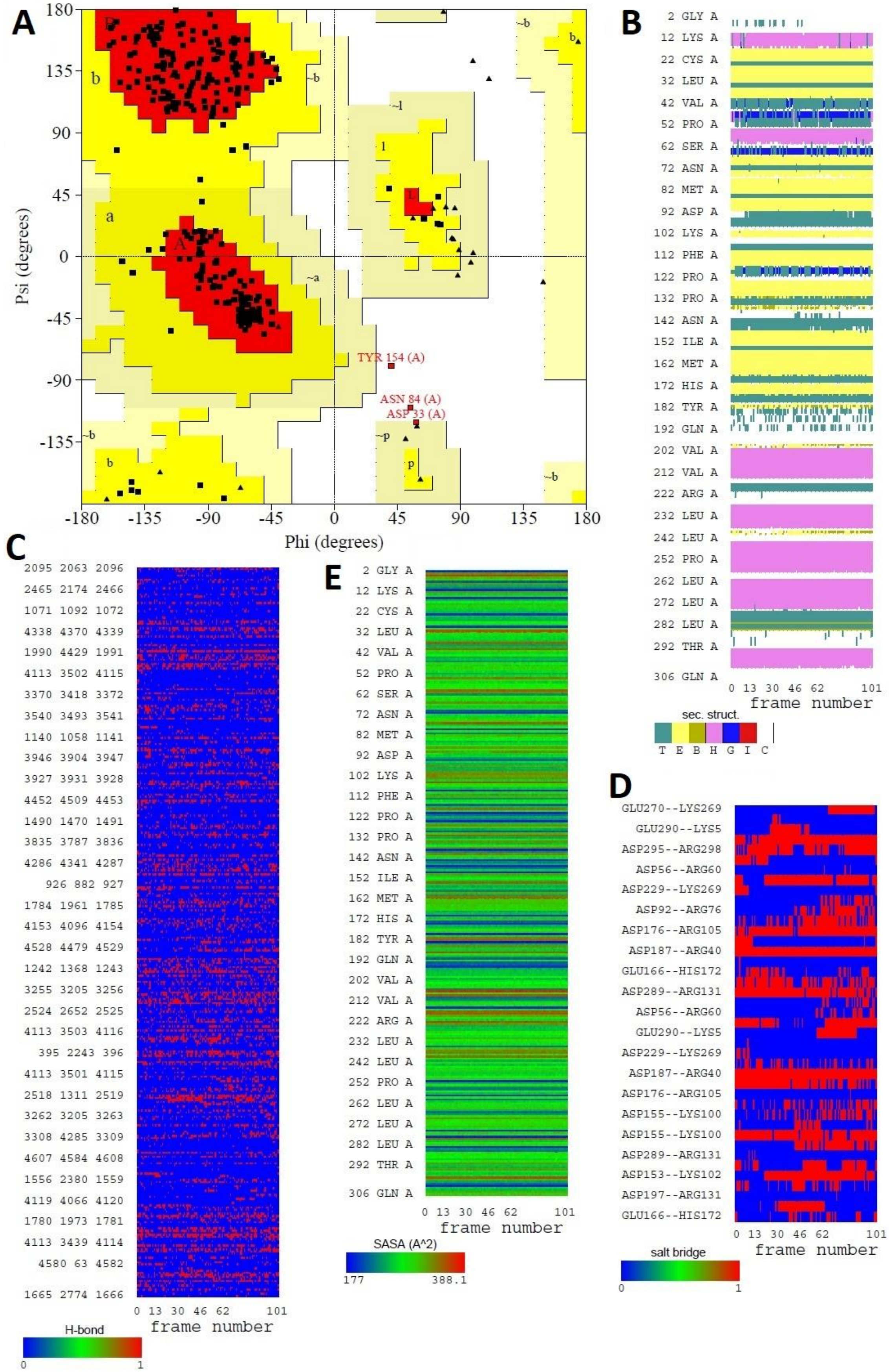

Fig. 6. (A) Ramachandran plot analysis of 7K3T-EWBC; VMD time series simulation analysis for 7K3T-EWBC: (B) secondary structures, (C) H-bond, (D) salt bridge interaction, and (E) SASA.

ISSN 2278–540X EISSN 2278–5396 I OPEN ACCESS

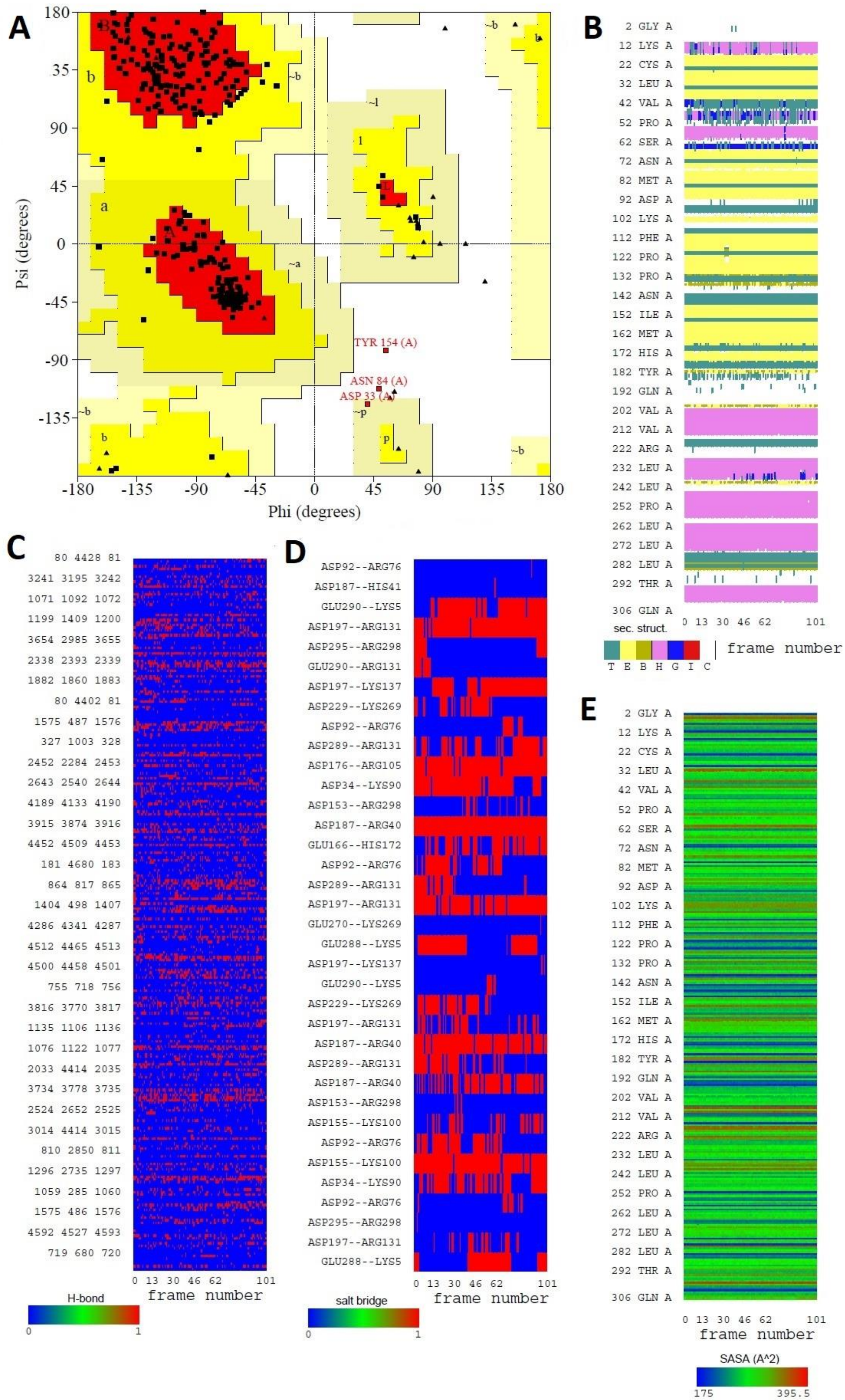

Fig. 7. (A) Ramachandran plot analysis of 7K3T-INMW; VMD time series simulation analysis for 7K3T-EWBC: (B) secondary structures, (C) H-bond, (D) salt bridge interaction, and (E) SASA.

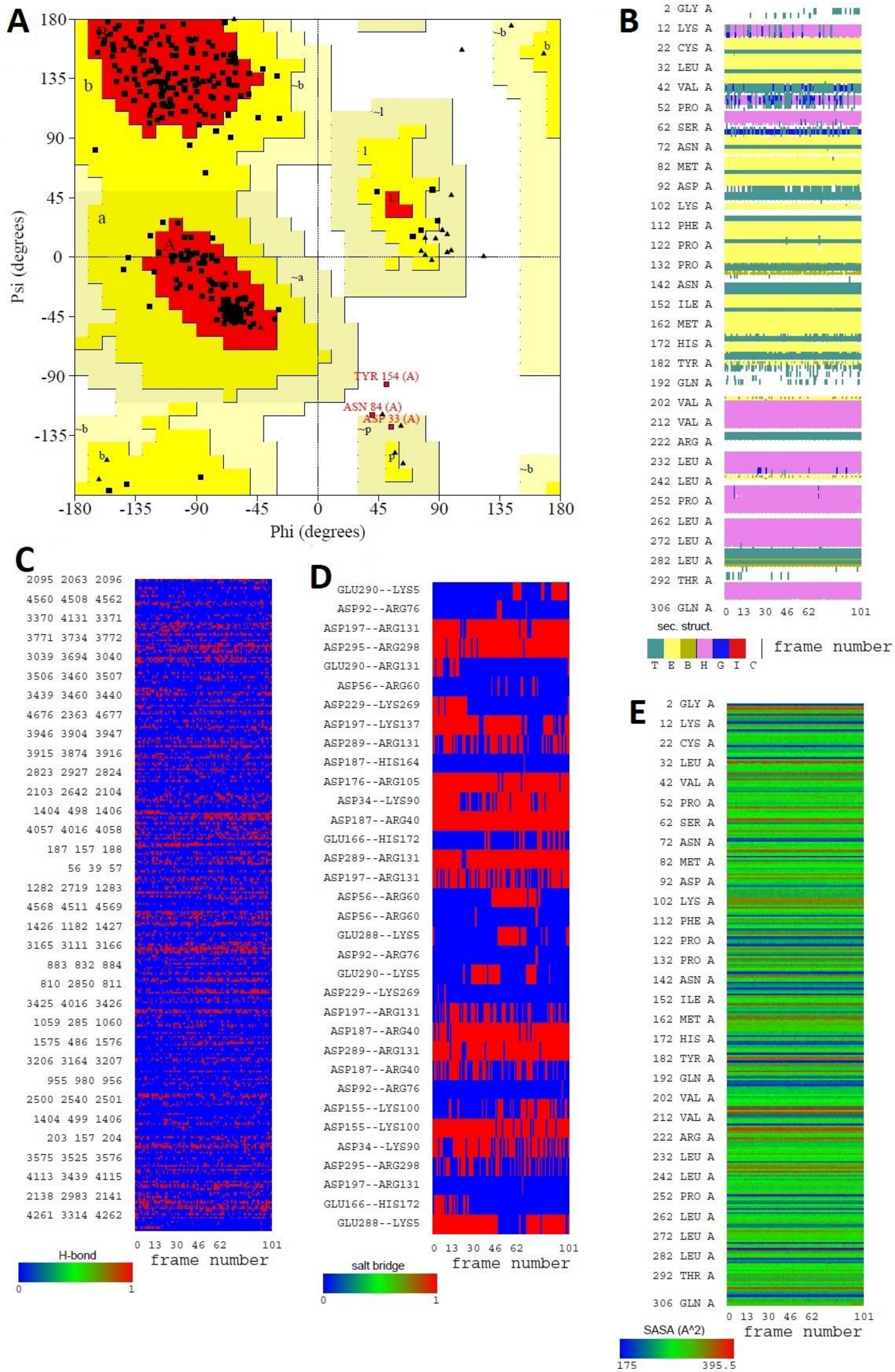

Fig. 8. (A) Ramachandran plot analysis of 7K3T-X7TW; VMD time series simulation analysis for 7K3T-EWBC: (B) secondary structures, (C) H-bond, (D) salt bridge interaction, and (E) SASA.

ISSN 2278–540X EISSN 2278–5396 I OPEN ACCESS

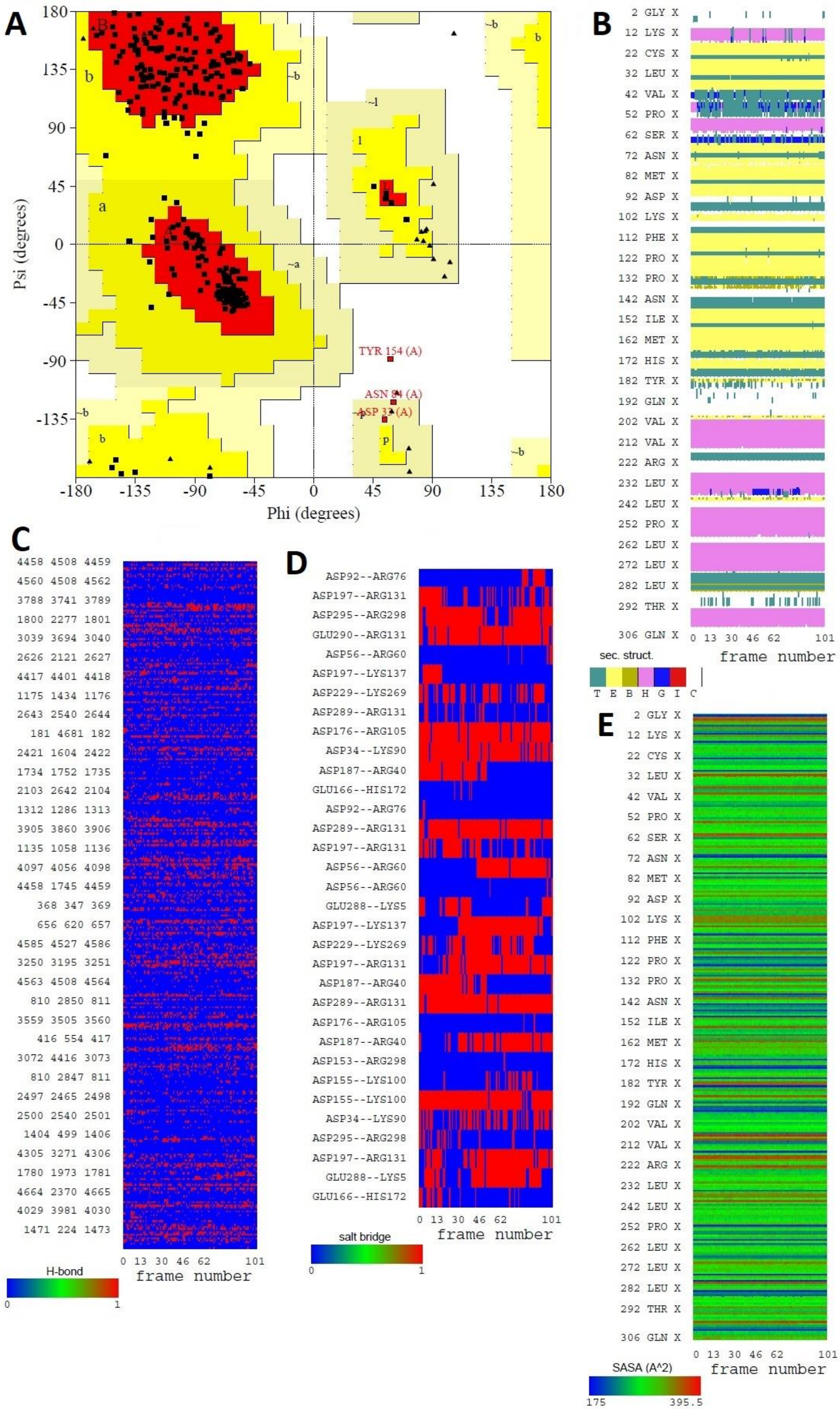

Fig. 9. (A) Ramachandran plot analysis of 7K3T; VMD time series simulation analysis for 7K3T-EWBC: (B) secondary structures, (C) H-bond, (D) salt bridge interaction, and (E) SASA.

VMD time series H-bond and salt bridge interaction

The MD simulation trajectory analysis of H-bonds, their occupancy percent in the structure, and salt bridge interaction for halo 7K3T in complex with EWBC (Fig. 6C and 6D), INMW (Fig. 7C and 7D), X7TW (Fig. 8C and 8D) and apo 7K3T (Fig. 9C and 9D) are explained later in the context of molecular interactions.

Solvent Accessible Surface Area of protein-ligand

The protein-ligand complexes were exposed to the solvent with an average area of 147-193 nm^2 (Table IV, Fig. 6E, 7E, 8E, 9E). The complex bearing polar molecules showed higher average area of 193 nm^2, compared to non-polar (150 nm^2) counterpart and combination of the two (149 nm^2) (Fig. 10A). The 7K3T contribution in SASA was ~ 2 nm^2 less than that of the protein-ligand complex. SASA per residue ranged 0.48-1.4 nm^2 with Arg217 (polar) and Phe223 (non-polar) as the major contributors (Table IV, Fig. 10B).

Table IV. Free energy of solvation (ΔG_{solv}), solvent accessible surface area (SASA) and residue area for the polar, non-polar and total residues of bound and unbound protein during MD simulation

Structure	Residue types	ΔG_{solv} (kJ/mol)	SASA (nm^2)	residue area (nm^2)
7K3T-EWBC	Non-polar	75.36 ± 0.45	150.28 ± 0.14	0.98 ± 0.6
	Polar	14.73 ± 0.37	193.77 ± 0.18	1.394 ± 0.6
	Total-protein	-34.97 ± 0.41	148.66 ± 0.19	0.48 ± 0.5
7K3T-INMW	Non-polar	74.98 ± 0.42	150.57 ± 0.13	0.98 ± 0.6
	Polar	11.83 ± 0.5	193.96 ± 0.21	1.395 ± 0.6
	Total-protein	-34.29 ± 0.38	149.98 ± 0.15	0.49 ± 0.5
7K3T-X7TW	Non-polar	75.39 ± 0.47	150.12 ± 0.14	0.98 ± 0.6
	Polar	13.49 ± 0.43	193.96 ± 0.16	1.395 ± 0.6
	Total-protein	-35.98 ± 0.44	149.92 ± 0.18	0.49 ± 0.5
7K3T	Non-polar	75.03 ± 0.45	150.58 ± 0.12	0.98 ± 0.6
	Polar	12.49 ± 0.44	191.44 ± 0.14	1.377 ± 0.6
	Total-protein	-37.05 ± 0.46	147.52 ± 0.14	0.48 ± 0.5

ΔG_{solv}: free energy of solvation (kJ/mol); SASA: solvent accessible surface area (nm^2); values expressed as mean ± SEM (standard error of mean)

ISSN 2278–540X EISSN 2278–5396 I OPEN ACCESS

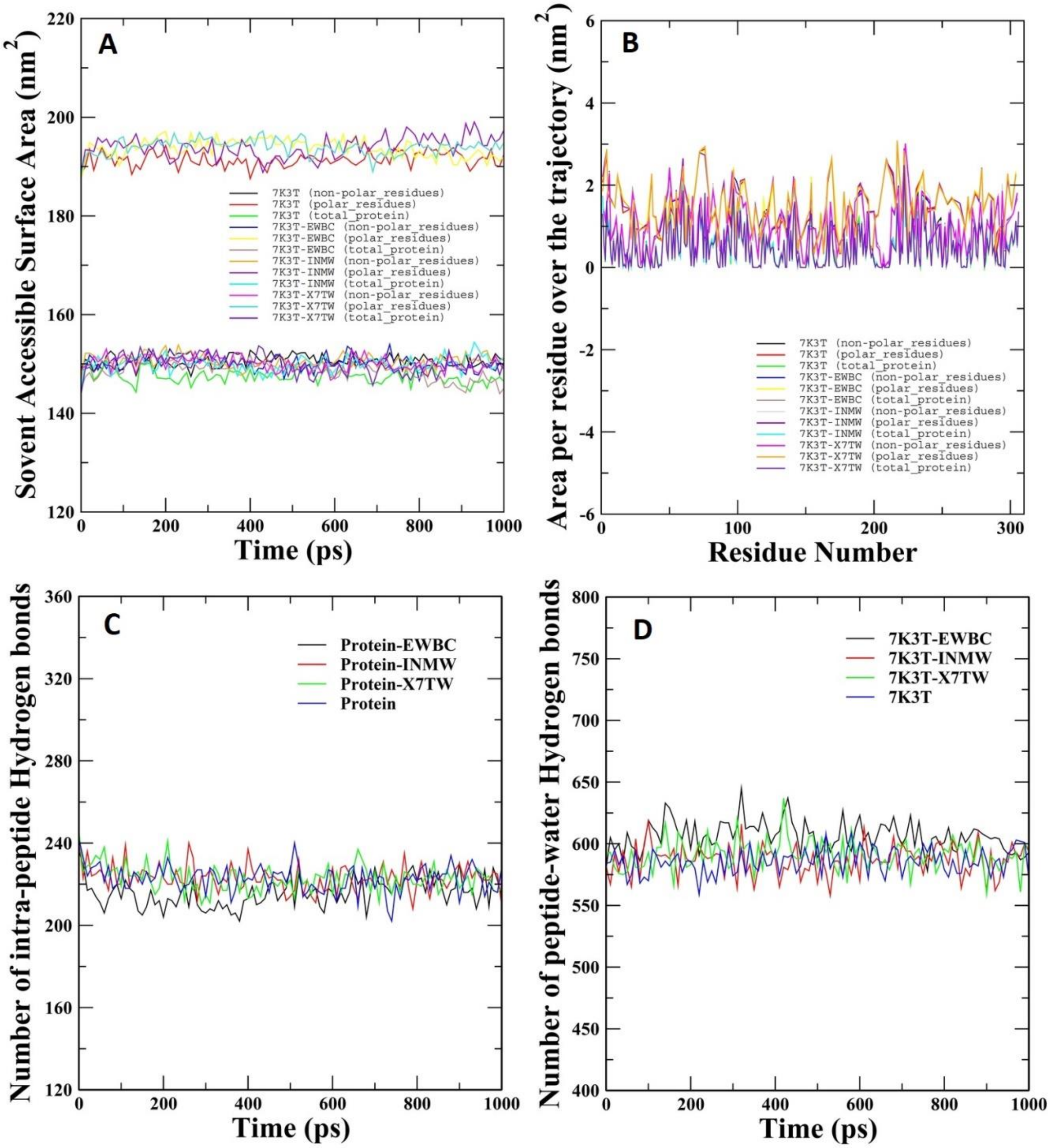

Fig. 10. SASA analysis: (A) about the polar, non-polar and total protein residues and (B) per residue; number of H-bonds: (C) intra-peptide and (D) peptide-water.

ISSN 2278–540X EISSN 2278–5396 I OPEN ACCESS

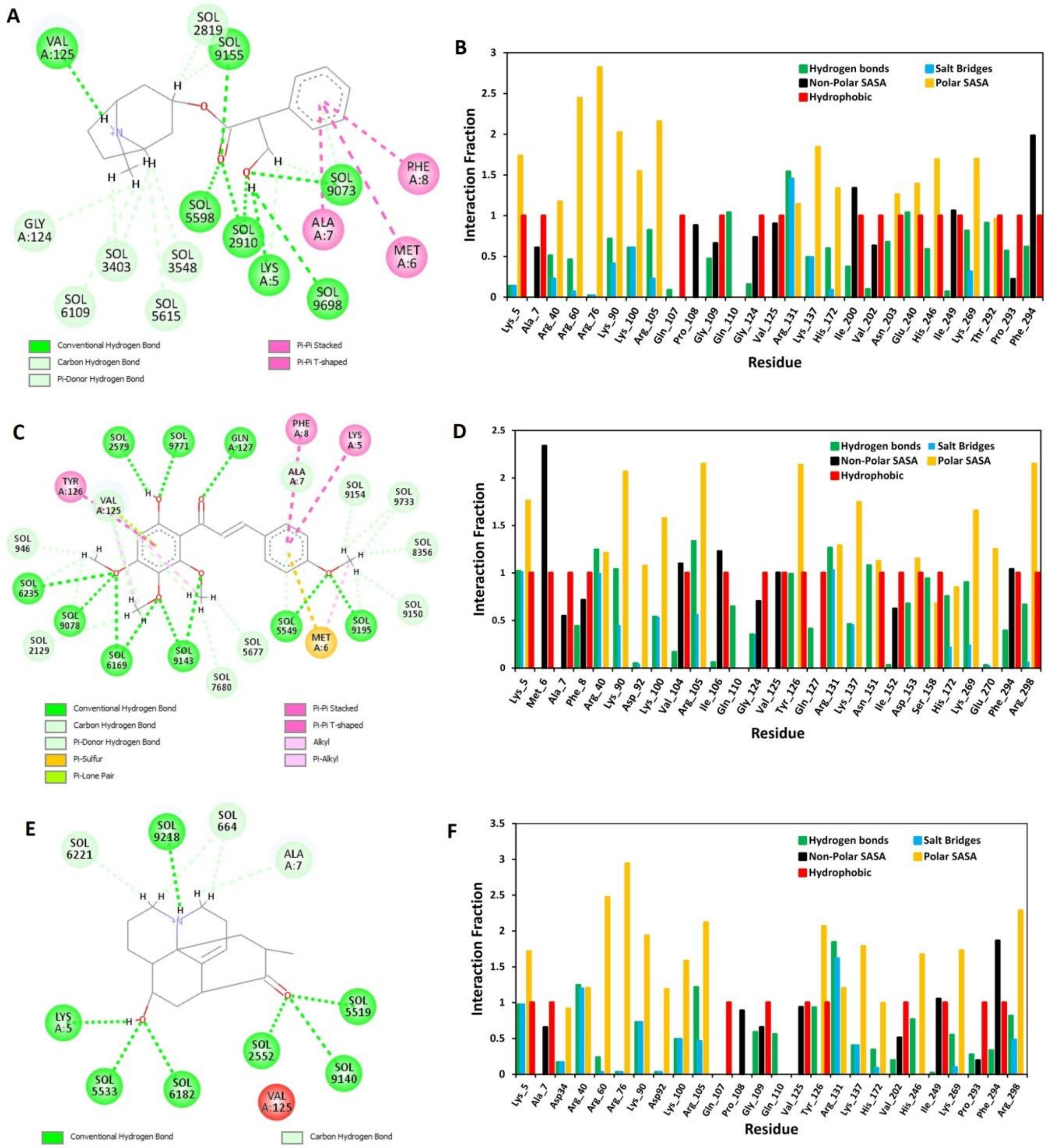

Fig. 11. 2D interaction of the simulated complex: (A) 7K3T-EWBC, (C) 7K3T-X7TW, (E) 7K3T-INMW; interaction fraction: (B) 7K3T-EWBC, (D) 7K3T-X7TW and (F) 7K3T-INMW.

Molecular interaction of 3CLpro with ligands after MD simulation

A large number of peptide-water H-bonds compared to intra-peptide H-bonds were found, due to the dissolution of solutes in large number of solvent molecules (Table III, Fig. 10C and 10D). The equilibrated 7K3T-EWBC complex exhibited two conventional H-bonds with Lys5 and Val125, two C-H bonds with Lys5 and Gly124, two hydrophobic interactions: π-π stacked (Ala7 and Phe8) and π-π T-shaped (Met6 and Ala7) (Fig. 11A and 11B). The 7K3T-INMW demonstrated one conventional H-bond with Gln127 and three C-H bonds with Val125 (Fig. 11C and 11D). In addition, 7K3T-INMW displayed one π-donor H-bond with Ala7, one π-S bond with Met6, π-lone pair with Val125, one π-π stacked (Ala7 and Phe8), three π-π T-shaped (Lys5 with Met6, Met6 with Ala7, Val125 with Tyr126), three alkyl bonds with Val125 and Met6, π-alkyl bond with Ala7. The 7K3T-X7TW showed one conventional H-bond with Lys5 and one C-H bond with Ala7 (Fig. 11E and 11F). The H-bond distance ranged 1.74 - 2.89 Å, and D-H···A angle ranged 150.45 - 164.04^0 (Fig. 11). The Arg40 of 7K3T donated H-atom to Asp187 in complex with X7TW and INMW with maximum 119.61% and 100% occupancies, respectively (Fig. 7C and 8C). Complexation with EWBC exhibited 88.24% maximum occupancy between Arg217 and Gly215, compared to the highest 82.35% occupancy for apo 7K3T between Arg131 and Asp289 (Fig. 6C and 9C). The carbon-hydrogen bond distance ranged 2.69 - 3.05 Å with bond angles ranging from 93.63 to 113.94^0. The hydrogen acceptors were Lys5 and Gly124 in 7K3T-EWBC, Val125 in 7K3T-INMW, and Ala7 in 7K3T-X7TW (Fig. 11). Seventeen salt-bridges were formed for each of 7K3T-EWBC-and 7K3T-INMW, while 7K3T-X7TW and apo 7K3T generated 16 and 15 salt bridges, respectively (Table III). Arg131 formed maximum number of salt bridges involving Asp197, Asp289, Glu290 both in presence and absence of complexation (Fig. 6D, 7D, 8D, 9D).

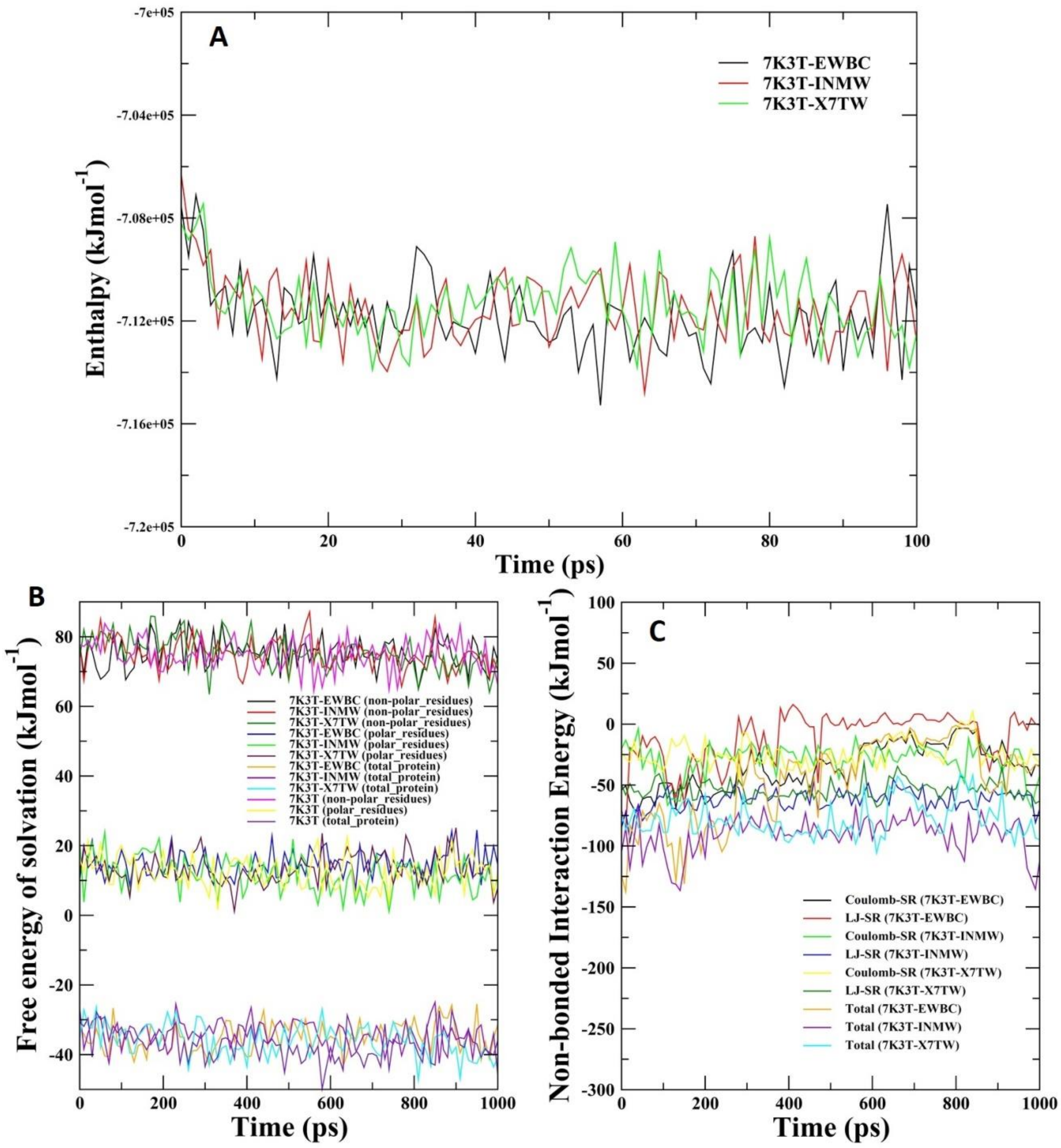

Fig. 12. MD simulation time-series energy components of protein-ligand complex: (A) enthalpy, (B) free energy change of solvation for polar, non-polar and total protein residues, and (C) non-bonded interaction energy.

Free energy calculation for 3CLpro ligand interaction

The enthalpy for apo and halo protein were -7.12×10^5 and -7.11×10^5 kJ/mol, respectively (Table III, Fig.12A). The free energy change of solvation, ΔG_{solv}, for the apo and halo protein are shown in Table IV and Fig. 11B. The ΔG_{solv} for polar residues were from 11.83 to 14.73 kJ/mol, for non-polar residues ~75 kJ/mol, and for combinations were from -37.05 to -35.98 kJ/mol (Fig. 12B).

The non-bonded interaction energy between the ligands and protein were quantified from the strength of short-range Coulombic (C-SR)/electrostatic energy and short-range Lennard-Jones (LJ-SR)/Van der Waals energy (Fig. 12C). The contribution of electrostatic and Van der Waals energy components, respectively, revealed a higher value for 7K3T-INMW (-28.64 kJ/mol and -62.33

ISSN 2278–540X EISSN 2278–5396 I OPEN ACCESS

kJ/mol), compared to that of 7K3T-X7TW (-24.34 kJ/mol and -53.87 kJ/mol) and 7K3T-EWBC (-11.59 kJ/mol and -35.44 kJ/mol) (Table III, Fig. 12C). The non-bonded interaction energy of 7K3T-INMW (-90.97 kJ/mol) was higher compared to that of the 7K3T-X7TW (-78.22 kJ/mol) and 7K3T-EWBC (-47.03 kJ/mol). The ΔG_{solv} was higher for 7K3T-X7TW (-35.98 kJ/mol) compared to 7K3T-EWBC (-31.93 kJ/mol) and 7K3T-INMW (-30.39 kJ/mol) (Fig. 12b).

4. DISCUSSION

The homeopathic medicines such as *Atropa belladonna*, *Eupatorium perfoliatum*, and *Lycopodium clavatum* are reported useful against various diseases, and might be repurposed in the management of COVID-19 associated symptoms[21-23]. The bioavailability radar representing optimal range of properties signifying the drug-likeness of compounds were[24-25]: lipophilicity (-0.7 < XLOGP3 < 5.0), size (150g/mol < MW < 500g/mol), polarity (20Å² < TPSA < 130Å²), solubility (log *S* (ESOL) < 6), flexibility (number of rotatable bonds < 9), and saturation (0.25 < fraction Csp3 < 1); values for our ligands ranged, respectively, from 1.00 to 3.77, 261.36 g/mol to 344.36 gm/mol, 40.54 Å² to 74.22 Å², -4.24 to -2.09, zero to 7, and 0.21 to 0.81, lying within the pink region. However, the INMW saturation value was slightly lower in terms of fraction csp3 (0.21), nevertheless, the bioavailability score for EWBC, INMW, and X7TW ligands, in our study, was 0.55, indicating their acceptability for oral administration[24]. In-silico toxicity by ADMET showed none of the ligands EWBC, INMW, and X7TW possessed potential hepatotoxicity or cytotoxicity except INMW AMES positive.

The prevailing interaction patterns governing protein-ligand molecular docking were 0.38% (12/32) hydrophobic interactions, 0.53 % H-bonds (17/32), and 0.09% (3/32) electrostatic bond. A model of a protein with docked ligand considers the bound state whereas desolvation plays a very important role, particularly with ionised or polar functional groups in molecular interaction necessitating characterization of dynamic interactions of protein-ligand complexes with MD simulation[26].

The MD simulation is an established bioinformatic approach for the investigation of the stability and spatio-temporal dynamic evolution of the protein-ligand complex at atomistic resolution[27]. The systems considered herein this study exhibited proper equilibration with respect to the temperature, pressure and density required for MD simulation. The position restraints applied to both apo and halo protein in our study did not impose any variation in the crystal and equilibrated structure for both RMSD and RMSF of backbone atoms after least square fit to backbone and ligand heavy atoms. Both apo and halo 7K3T exhibited good quality model evident from 90.2% residues falling in the most favored regions in Ramachandran plot. The key amino acid players in protein-ligand interactions in the current study were Lys5, Met6, and Ala7 positioned in the coils, and Gly124 and Val125 positioned in the β-sheets. The SASA profile of protein-ligand complex remained stable throughout the process of simulation similar to the earlier findings[28].

Molecular interaction of 7K3T with the ligands after MD simulation displayed hydrophobic bonds occurring majorly, with 4.0 Å cut-off distance, between aliphatic carbon of protein and aromatic carbon of ligands, because of the presence of aromatic rings in small ligand molecules, wherein the mostly involved residues were Leu, Val, Ile, and Ala in the side-chains, as reported earlier also[29]. We found the involvement of Met6, Ala7, Phe8, and Tyr126 in hydrophobic interaction of EWBC and/or INMW with 7K3T, while in 7K3T-X7TW complex, no hydrophobic interaction was detected. The H-bond was the second most frequent interaction type, followed by π-π stacking involving the aromatic ring of Phe8 in 7K3T-EWBC, and 7K3T-INMW, in addition to Tyr126 in the latter.

Binding free energy calculation for some selected natural compounds with 3CLpro showed values ranging from −70.41 kcal/mol (rutin) to −38.92 kcal/mol (podocarpusflavon-B)[6], −42.42 kJ/mol (calycin), and −57.85 kJ/mol (rhizocarpic acid)[30], which were higher compared to our findings. Herein, the net binding free energy in 7K3T-INMW was more favorable than 7K3T-X7TW and 7K3T-EWBC. Van der Waals interactions mainly contributed to the net binding free energy, followed by free energy of solvation for polar non-polar combined residues, and electrostatic free energy component. Thus, 7K3T-INMW represented lowest net binding free energy (-121.36 kJ/mol) conferring INMW greater receptor binding potentiality. Whereas, other ligands i.e., X7TW (-114.17 kJ/mol), and EWBC (-78.96 kJ/mol) also demonstrated favorable binding free energies with SARS-CoV-2 3CLpro, suggesting that all the ligand molecules achieved thermodynamically stable and strong complex with the SARS-CoV-2 3CLpro.

The current study authenticated, by MD simulation and docking analysis, the inhibitory property of bioactive antiviral phytocompounds L-hyoscyamine, eupatorium and alkaloid L27, due to their good binding affinities and energetically stable complex formation potentiality with 3CLpro of SARS-CoV-2. The physicochemical and pharmacokinetic properties interpreted with ADMET profile and bioavailability score indicated their suitability as potential drug candidates against COVID-19.

ISSN 2278–540X EISSN 2278–5396 I OPEN ACCESS

Author's contribution

Both the authors Manisha Mandal and Shyamapada Mandal jointly designed the study, analysed and interpreted the data, discussed and wrote the manuscript.

Ethical approval

Not applicable.

Funding:

This study has not received any external funding.

Conflict of Interest:

The authors declare that there are no conflicts of interests.

Data and materials availability:

All data associated with this study are present in the paper.

REFERENCES AND NOTES

1. Behera SK, Mahapatra N, Tripathy CS, Pati S. Drug repurposing for identification of potential inhibitors against SARS-CoV-2 spike receptor-binding domain: An in silico approach. *Indian J Med Res* 2021; *153*: 132-43.
2. Li X, Geng M, Peng Y, Meng L, Lu S. Molecular immune pathogenesis and diagnosis of COVID-19. *J Pharm Analys* 2020; *10*: 102-8.
3. Bzowka M, Mitusinska K, Raczynska K, Samol A, Tuszynski JA, Gora A. Structural and evolutionary analysis indicate that the SARS-COV-2 Mpro is a challenging target for small-molecule inhibitor design. *Int J Mol Sci 2020*; 21: 3099.
4. Li G, Clercq E De. Therapeutic options for the 2019 novel coronavirus (2019-nCoV). *Nat Rev Drug Discov* 2020 *19*: 149-50.
5. Amaresh M, Yamini P, Anuj K, Mishra KS, Tripathi V. Natural compounds as potential inhibitors of SARS-CoV-2 main protease: an in-silico study. *Asian Pac J Trop Biomed* 2021; *11*: 155 - 63.
6. Bharadwaj S, Dubey A, Yadava U, Mishra SK, Kang SG, Dwivedi VD. Exploration of natural compounds with anti-SARS-CoV-2 activity via inhibition of SARS-CoV-2 Mpro. *Brief Bioinformatics* 2021 *22*: 1361-77.
7. Lokhande KB, Doiphode S, Vyas R, Swamy K. Molecular docking and simulation studies on SARS-CoV-2 Mpro reveals mitoxantrone, leucovorin, birinapant, and dynasore as potent drugs against COVID-19, *J Biomol Struct Dyn* 2020 Aug: 1 - 12.
8. Murugan NA, Pandian CJ, Jeyakanthan J. Computational investigation on *Andrographis paniculata* phytochemicals to evaluate their potency against SARS-CoV-2 in comparison to known antiviral compounds in drug trials. *J Biomol Struct Dyn* 2020 Jun: 1 - 12.
9. Gold P. The AIH COVID-19 data collection project. *Am J Homeopath Med* 2020. Available from: https://homeopathyusa.org/journal/ajhm-journal/ajhm-issues-2020/the-aih-covid-19-data-collection-project.html, accessed on April 1, 2021.
10. Bekker A. Some common remedies in pneumonia and COVID-19: with indications especially for characteristics of cough. *Am J Homeopath Med* 2020; *113*. Available from: *https://homeopathyusa.org/journal/ajhm-journal/ajhm-issues-2020/some-common-remedies-in-pneumonia-and-covid-19.html, accessed on April 1, 2021.*
11. *Adler UC, Adler MS, Hotta LM, Padula AEM, deT Cesar A, Diniz JNM*, et al. *Homeopathy for Covid-19 in primary care: a structured summary of a study protocol for a randomized controlled trial. Trials 2021; 22: 109.*
12. Lipinski CA. Lead- and drug-like compounds: the rule-of-five revolution. *Drug Discov*. *Today*: *Technol* 2004; *1:* 337 - 41.
13. Hosseini M, *Chen W, Xiao D, Wang C.* Computational molecular docking and virtual screening revealed promising SARS-CoV-2 drugs. *Precision Clinic Med 2020; 4: 1-16.*
14. Vanommeslaeghe K, MacKerell Jr AD. Automation of the CHARMM general force field (CGenFF) I: bond perception and atom typing. *J Chem Inf Model* 2012; *52*: 3144 - 54.
15. Vanommeslaeghe K, Hatcher E, Acharya C, Kundu S, Zhong S, Shim J, et al. CHARMM general force field: a force field for drug-like molecules compatible with the CHARMM all-atom additive biological force field. *J Comput Chem* 2010; *31*: 671 - 90.
16. Berendsen HJ, van der Spoel D, van Drunen R, GROMACS: A message passing parallel molecular dynamics implementation. *Comput Phys Commun* 1995; *91*: 43 - 56.

ISSN 2278–540X EISSN 2278–5396 I OPEN ACCESS

17. Abraham MJ, Gready JE. Optimization of parameters for molecular dynamics simulation using smooth particle-mesh Ewald in GROMACS 4.5. *J Comput Chem* 2011; *32*: 2031 - 40.
18. Parrinello M, Rahman A. Polymorphic transitions in single crystals: a new molecular dynamics method. *J Appl Phys* 1981; *52*: 7182 - 90.
19. Hockney RW, Goel SP, Eastwood J. Quiet high resolution computer models of a plasma. *J Comp Phys* 1974; *14:* 148 - 58.
20. Kollman PA, Massova I, Reyes C, Kuhn B, Huo S, Chong L, et al. Calculating structures and free energies of complex molecules: combining molecular mechanics and continuum models. *Acc Chem Res* 2000; *33*: 889 - 97.
21. *Hoover T.* Belladonna: A clinical snapshot. *Am Assoc Homeopath Pharam* 2017. Available from: *https://www.theaahp.org/articles/belladonna-clinical-snapshot/*, accessed on April 6, 2021.
22. Jatoliya A, John J, Shaha SR, Sharma R, Kumawat P. Role of *Eupatorium perfoliatum* in the cases of dengue fever. *European J Mol Clinic Med 2020; 7*: 1794 – 6.
23. *Li X, Kang M, Ma N, Pang T, Zhang Y, Jin H, et al. Identification and analysis of chemical constituents and rat serum metabolites in Lycopodium clavatum using UPLC-Q-TOF/MS combined with multiple data-processing approaches. Evidence-Based Complement Alternat Med 2019 Jul: 1 - 8.*
24. Daina A, Michielin O, Zoete V. SwissADME: A free web tool to evaluate pharmacokinetics, drug-likeness and medicinal chemistry friendliness of small molecules. *Sci Rep* 2017; 7: 42717.
25. Martin YCA. Bioavailability score. *J Med Chem* 2005; 48: 3164 - 70.
26. Ganesan A, Coote ML, Barakat K. Molecular dynamics-driven drug discovery: leaping forward with confidence. *Drug Discov Today* 2017; *22*: 249 - 69.
27. N.C. Benson, V. Daggett, A comparison of multiscale methods for the analysis of molecular dynamics simulations, *J Phys Chem B* 2012; *116:* 8722 - 31.
28. Chandra Babu TM, Sivarathri SR, Baki VB, Savita D, Aluru R, Thirunavakkarasu S, et al. Molecular docking, molecular dynamic simulation, biological evaluation and 2D-QSAR analysis of flavonoids from *Syzygium alternifolium* as potent anti-*Helicobacter pylori* agents, *RSC Adv* 2017; *7*: 18277 - 92.
29. de Freitas RF, Schapira M. A systematic analysis of atomic protein-ligand interactions in the PDB. *Med Chem Commun* 2017; *8*: 1970 - 81.
30. Joshi T, Sharma P, Joshi T, Pundir H, Mathpal S, Chandra S. Structure-based screening of novel lichen compounds against SARS *Coronavirus* main protease (Mpro) as potentials inhibitors of COVID-19. *Mol Diversity* 2020 Jun: 1 - 13.

ISSN 2278–540X EISSN 2278–5396 I OPEN ACCESS